King's Research Portal

Document Version
Peer reviewed version

Link to publication record in King's Research Portal

Artefact-free high density localization microscopy analysis

Richard J. Marsh[1], Karin Pfisterer[1], Pauline Bennett[1], Liisa M. Hirvonen[1], Mathias. Gautel[1], Gareth E. Jones[1], Susan Cox [1]

[1]Randall Centre for Cell and Molecular Biophysics, King's College London, Guy's Campus, Lon-don, SE1 1UL, UK

Corresponding author: susan.cox@kcl.ac.uk

High density analysis methods for localization microscopy increase acquisition speed but produce artefacts. We demonstrate that these artefacts can be eliminated by combining a Haar wavelet kernel (HAWK) analysis with standard single frame fitting. We tested the performance on synthetic, fixed cell and live cell data, demonstrating that HAWK pre-processing gives reconstructions which reflect the structure of the sample, enabling high speed, artefact-free super-resolution in live cells.

Localization microscopy methods such as photoactivatable localization microscopy (PALM)[1] and stochastic optical reconstruction microscopy (STORM)[2] rely on the localization of small numbers of well-separated fluorophores in each frame of the raw dataset. Consequently data acquisition is slow, and generally limited to examination of fixed cells. Severe artefacts including false structure, collapse of multiple features into one, and artificial sharpening are possible if the activation density of fluorophores is too high[3,4,5]. However, assessing the activation density is extremely challenging, particularly since the density of fluorophores often varies considerably across the sample. Currently the only assessment methods for the raw data are subjective visual checks or time consuming post-acquisition reclassification[5]. Resolution assessment methods including Fourier Ring Correlation (FRC)[6] will report artificial sharpening as enhanced resolution[5,6], and are therefore unsuitable to assess data which may contain mis-localizations.

A number of methods have been developed to allow for overlapping fluorophores, to enable faster acquisition and therefore live cell imaging. These methods, including multi-emitter fitting[7,8], compressed sensing[9], BALM[10], SOFI[11], 3B[12], and SRRF[13], either model patches of a single frame as arising from a number of overlapping fluorophores, use temporal fluctuations to enhance resolution, or use a combination thereof. However, if the activation density is too high, artefacts will still appear. All these methods suffer from the same fundamental problem as low-density fitting: there is no way to tell if the activation density is so high that there will be artefacts in the analysed image.

Previous evaluations of high-density methods have reported resolutions of 50-100 nm. However, these methods can artificially collapse structures up to 200nm apart into a single structure, as can be seen in Fig. 1, and Supplementary Figs 1 and 2. Simulation of pairs of lines at an angle to each other demonstrated the collapse of two structures into one by most high-density methods, and artefacts in all of the generated images (Supplementary Fig. 1).

Consequently there is an urgent need for a high-density analysis method that will produce results which reliably reflect the true underlying structure of the sample. Such a method would

allow high-speed live cell localization microscopy to be carried out with full confidence that the results reflect the sample structure and would allow those carrying out fixed cell experiments to check that their data does not contain any areas unsuitable for single-emitter fitting.

Here we present Haar wavelet kernel (HAWK) analysis, a method of pre-processing localization microscopy data which takes generates a dataset several times the length of the original, with a much lower density of emitters. In effect this new dataset is the original dataset with several different levels of temporal bandpass filtering applied. This pre-processing allows fluorophores to be separated from each other by their blinking behaviour before localization analysis is carried out, and has the advantage that it can be paired with any other localization analysis method which does not model the fluorophore blinking properties.

The performance of HAWK on simulated structures is shown in Fig. 1a & b. HAWK analysis followed by single or multi emitter ThunderSTORM[14] fitting is able to retrieve linear structures from data on which every other method we have tested fails. Furthermore, it does not pinch together approaching pairs of lines (Supplementary Fig. 1) or collapse circular structures to a dot smaller than the true size (Supplementary Fig. 2), whereas these effects are observed for other methods around the 200nm lengthscale when the excitation density is very high. There are two exceptions: 3B performs well on circular structures and does not collapse them to a point, while SOFI displays relatively little artificial sharpening. However, the SOFI results demonstrate a disadvantage of methods which use nonlinear processing (such as SOFI and SRRF) on the image. Intensity differences in the image are magnified, leading to information from lower intensity areas being lost. In extended two dimensional structures methods other than HAWK produce false texture (Supplementary Fig. 3), while if there are out-of-focus fluorophores present the performance of all methods are degraded but HAWK still does not show artificial sharpening (Supplementary Fig. 4), nor is it effected by experimentally realistic levels of sample drift (Supplementary Fig. 4)[14,15].

After HAWK analysis, low-density algorithms produce results on simulated data which replicate the ground truth structure. Artificial sharpening, pinching, false structure and collapse to a single narrow structure do not appear (for varying line spacings and excitation densities see Supplementary Fig. 5). There are two trade-offs for this substantial increase in accuracy. First, there a slight decrease in the precision of the localization fits (around 10nm degradation in resolution compared to the Cremer Rao lower bound for molecule intensities and background levels typical for an experiment), giving a slightly larger scatter around the structure (Supplementary Fig. 6). Second, noise-induced single-pixel events are fitted by some algorithms (however, these can easily be filtered out, see Methods and Supplementary Note).

Simulations, although useful, may not capture the behavior of a real experiment. We were able to verify our results against two known biological structures. The antibody T12 binds to an epitope of the sarcomeric protein titin in myofibrils, while the antibody M8 binds to an epitope of titin at the M-band. Immunoelectron microscopy studies using pre-embedding labelling located T12 to a pair of lines to either side of the Z-disc separated by 160-200nm[16,17], and M8 to lines separated by 96±5 nm[18]. Results from high-density imaging of both T12 and M8 (Fig. 1, Supplementary Fig. 7 for alternative SRRF parameters, Supplementary Fig. 8 for raw and filtered frames, Supplementary Table 1 for molecule identification at different filter levels) show the same effects as the simulations; all methods except HAWK analysis fail to clearly separate the two lines (Fig 1f,j,m Supplementary Fig. 9). Note that these lines are projections of the 3D structure into two dimensions, so the imaging of these structures is compromised by the fact that

the myofibrils are not aligned perfectly vertically, and are not completely rigid. With HAWK filtering, single emitter ThunderSTORM fitting can separate pairs of lines (Fig. 1i,j,l,m). The spacing of the lines observed with HAWK (160 nm for T12, 87 nm for M8) was confirmed with subsequent low-density imaging (Fig. 1c,j, Supplementary Fig. 9), and is consistent with electron microscopy results. HAWK can also be used to improve the performance of other high-density methods, such as SOFI and SRRF (Supplementary Fig. 10). We have also tested HAWK on DNA origami structures, with a spacing of 50nm, and show that HAWK allows these structures to be resolved when other methods fail (see Supplementary Figs 11 and 12). This shows that HAWK can resolve structures significantly below the diffraction limit even at very high activation densities.

Although the primary advantage of high-density methods is that they enable live cell imaging, evaluating the performance of algorithms in live cells is challenging as there is very rarely ground truth information about the sample structure. To evaluate HAWK, we have taken both low-density and high-density localization data for two different live cell structures. To do this we used photoswitchable fluorescent proteins (mEOS2 and mEOS3.2) and imaged them in both the switched (low-density) and unswitched (high-density) channels. First we imaged podosome rings, which are approximately circular structures around 500 nm in diameter in which we expressed a partial mEOS3.2-talin construct that localises to the ring of the podosome[19]. Low-density (Fig. 2a) and then high-density (Fig. 2b-e) localization data was taken (see f-j for high magnification images).

The results provide a stark illustration of how challenging artefacts can be to identify by the naked eye. In isolation, both the multi-emitter ThunderSTORM (ME-TS) (Fig. 2b,g) and the SRRF (Fig. 2d,i) appear to be better reconstructions than the HAWK, with sharper features and lower background. However, the low-density result reveals this to be a result of artificial sharpening. In addition, parts of the podosomes disappear when using ME-TS and SRRF (for examples see red and white arrows in Figs 2f-j), and the appearance of strand-type structures is altered (for examples see blue arrows in Figs 2f-j). The SOFI image is not sharpened but the structures are shadowed, the background contains artificial texture, the strand-type feature is not visible and the resolution is relatively low (see also Supplementary Fig. 13). In contrast, the HAWK processing, followed by single emitter fitting (Fig. 2e,j), yields an image very similar to the low-density result, with minor differences in intensity due to remodelling over the several minutes required for the low-density acquisitions. This can be demonstrated by summing multiple frames of the low density data to create a higher density dataset, and then using HAWK. This yields an intensity distribution very similar to the low density data, as expected (see Supplementary Fig. 14).

Secondly we examined focal adhesions. These are structures with a size between 500nm and several microns, with adhesion, signalling and force transmitting proteins present across the whole structure[20]. We imaged vinculin labelled with mEOS2, and simultaneously imaged both the switched and unswitched states of the fluorophore. This allowed us to collect high-density and low-density data simultaneously, giving us a ground truth structure to compare against our high-density results (See Figure 2k). It should be noted that due to the long collection times required for this type of structure the low density image is probably density limited in resolution (see Supplementary Figure 14 for results from summed low density frames). TS-ME (Fig. 2l) and SOFI (Fig. 2m) both produced results with substantial artificial sharpening and distortion. SRRF (Fig. 2n) exhibits less shape distortion, but has a very high background, texture at around

a 100nm length scale, and substantial fixed pattern noise (similar to Supplementary Fig. 3). In contrast, HAWK processed data shows great similarity to the low density ground truth (Fig. 2o).

Resolution is challenging to assess in localization microscopy, though from our simulations and experiments we can confidently say that HAWK results exhibit minimal degradation compared to equivalent low density data. We assessed resolution with a precision-based calculation[21,14], which for live cell results gave values between 44 and 73 nm, and FRC[6]. For live cell experiments the FRC resolution values varied strongly with structure (from 63 nm to 160 nm), but for fine structure (such as the focal complexes shown in Supplementary Figure 15), the value was 72±6 nm for a 4 s (400 frame) acquisition (the precision-based measure for the same area was 47 nm). For comparison, SIM and iSIM fixed cell experiments gave FRC values of 160 nm. Therefore when imaging in live cells HAWK can be expected to outperform SIM and iSIM by a factor of more than 2.

Reliable data processing which can be used with confidence by those not expert in analysis is a prerequisite for carrying out research using super-resolution microscopy. HAWK analysis gives that reliability, boosting resolution and accuracy of results for high-density data and, most importantly, giving results which the user can be confident do not contain artefactual features, at the cost of only a few seconds of pre-processing for a typical dataset. We have made it available as an ImageJ plugin (Supplementary Software).

Acknowledgements

Author Contributions

R.J.M. and S.C. conceived and designed the analysis and experiments. L.M.H. created the mEOS3.2-talin construct with assistance and advice from G.E.J., L.M.H. prepared the podosome samples, P.B. prepared the psoas myofibril samples, M.G. prepared the cardiac myofibril samples, and K.P. prepared the focal adhesion samples. R.J.M carried out the analysis and experiments. R.J.M, G.E.J. and S.C. discussed the results and prepared the manuscript and all authors revised the manuscript.

Competing Financial Interests

King's College London has filed a patent that includes portions of the research described in this manuscript, whose value may be affected by this publication (UK Patent Application No. 1800026.5).

Editor's summary

Pre-processing localization microscopy datasets using Haar wavelet kernel (HAWK) analysis enables artefact-free analysis of high density data for improved fixed and live-cell super-resolution microscopy.

References (main text)

1. Betzig, E. et al. Imaging intracellular fluorescent proteins at nanometer resolution. Science 313, 1642–1645 (2006).

2. Rust, M., Bates, M., and Zhuang, X. Sub-diffraction-limit imaging by stochastic optical re-construction microscopy (STORM). Nature Methods 3, 793–796 (2006).

3. Burgert, A., Letschert, S., Doose, S., and Sauer, M. Artifacts in single-molecule localization microscopy. Histochemistry and Cell Biology 144, 123–131 (2015).

4. Sage, D. et al. Quantitative evaluation of software packages for single-molecule localization microscopy. Nature Methods 12, 717–724 (2015).

5. Fox-Roberts, P. et al. Local dimensionality determines imaging speed in localization microscopy. Nature Communications 8, 13558 (2017).

6. Nieuwenhuizen, R. P. J. et al. Measuring image resolution in optical nanoscopy. Nature Methods 10, 557–562 (2013).

7. Huang, F., Schwartz, S., Byars, J., and Lidke, K. Simultaneous multiple-emitter fitting for single molecule super-resolution imaging. Biomedical Optics Express 2, 1377–1393 (2011).

8. Holden, S., Uphoff, S., and Kapanidis, A. DAOSTORM: an algorithm for high- density super-resolution microscopy. Nature Methods 8, 279–280 (2011).

9. Zhu, L., Zhang, W., Elnatan, D., and Huang, B. Faster STORM using compressed sensing. Nature Methods 9, 721–723 (2012).

10. Burnette, D. T., Sengupta, P., Dai, Y., Lippincott-Schwartz, J., and Kachar, B. Bleaching/blinking assisted localization microscopy for superresolution imaging using standard fluorescent molecules. Proc. Nat. Acad. Sci. 108, 21081–21086 (2011).

11. Dertinger, T., Colyera, R., Iyera, G., Weissa, S., and Enderleind, J. Fast, background-free, 3D super-resolution opticalfluctuation imaging (SOFI). Proc. Natl. Acad. Sci. 106, 22287–22292 (2009).

12. Cox, S. et al. Bayesian localization microscopy reveals nanoscale podosome dynamics. Nature Methods 9, 195–200 (2012).

13. Gustafsson, N. et al. Fast live-cell conventional fluorophore nanoscopy with ImageJ through super-resolution radial fluctuations. Nature Communications 7, 12471 (2016).

14. Ovesny,´ M., Kˇr´ızek,ˇ P., Zdenek,ˇ J. B., Svindrych, and Hagen, G. M. ThunderSTORM: a com-prehensive ImageJ plug-in for PALM and STORM data analysis and super-resolution imaging. Bioinformatics 30, 2389–2390 (2014).

15. Henriques, R. et al. QuickPALM: 3d real-time photoactivation nanoscopy image processing in ImageJ. Nature Methods 7, 339–340 (2010).

16. Furst,¨ D. O., Osborn, M., Nave, R., and Weber, K. The organization of titin filaments in the half-sarcomere revealed by monoclonal antibodies in immunoelectron microscopy: a map of ten nonrepetitive epitopes starting at the z line extends close to the m line. Journal of Cell Biology 106, 1563 (1988).

17. Trombitas,´ K., Jin, J.-P., and Granzier, H. The mechanically active domain of titin in cardiac muscle. Circulation Research 77, 856–861 (1995).

18. Obermann, W. M. et al. The structure of the sarcomeric m band: Localization of defined domains of myomesin, m-protein and the 250-kd carboxy-terminal region of titin by immuno-electron microscopy. The Journal of Cell Biology 134, 1441 (1996).

19. Rafiq, N. B. M. et al. Podosome assembly is controlled by the GTPase ARF1 and its nucleotide exchange factor ARNO. The Journal of Cell Biology 216(1), 181–197 (2017).

20. Geiger, B., P.Spatz, J., and Bershadsky, A. D. Environmental sensing through focal adhesions. Nature Reviews Molecular Cell Biology 10, 21–33 (2009).

21. Thompson, R., Larson, D., and Webb, W. Precise nanometer localization analysis for individ-ual fluorescent probes. Biophys. J. 82, 2775–2783 (2002).
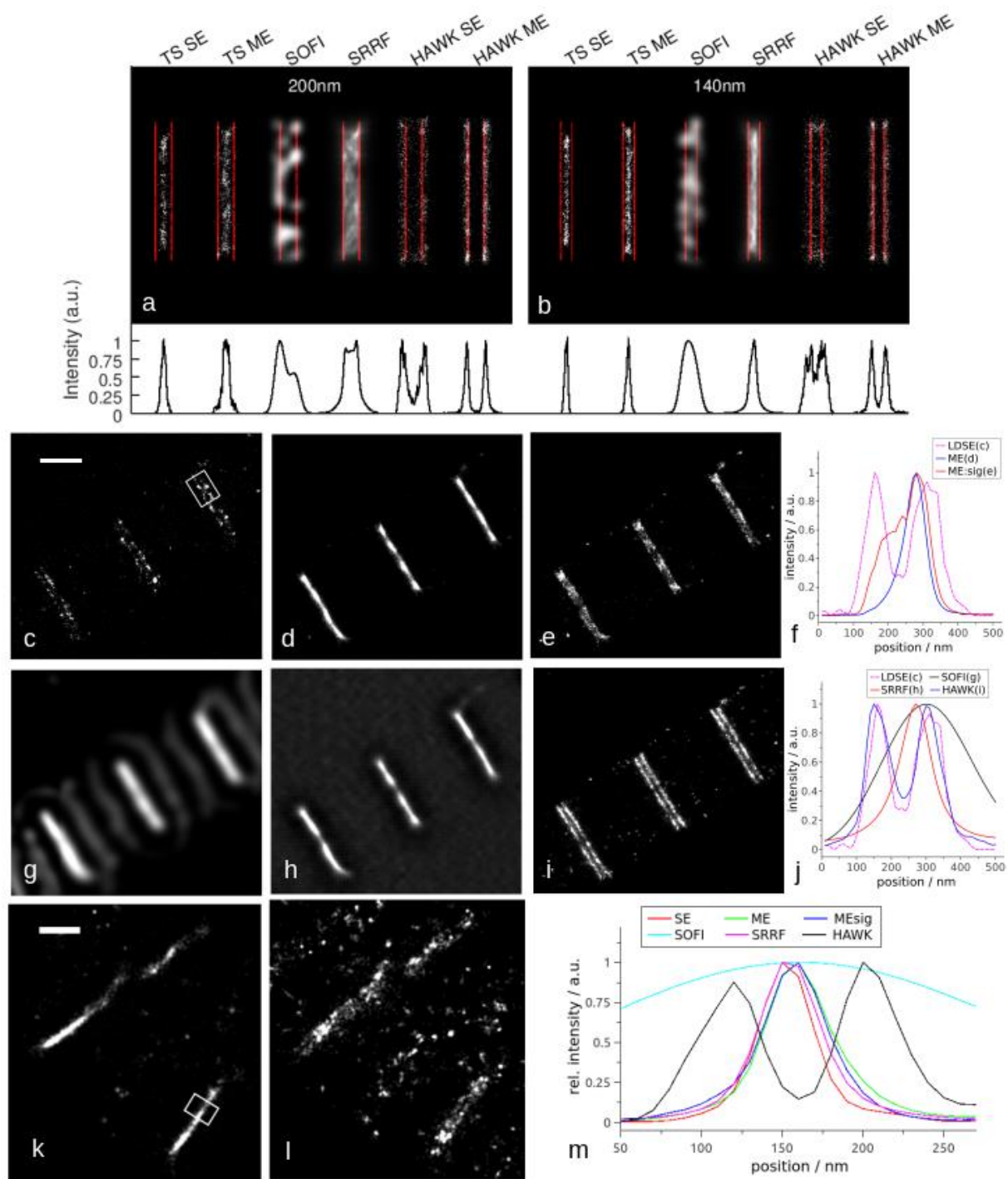
Figure 1 HAWK processing improves results and removes artefacts in localization microscopy. Simulations of parallel lines separated by a) 200nm and b) 140nm. Methods tested are, from left to right, single emitter fitting (ThunderSTORM) multi-emitter fitting (ThunderSTORM), 4th order SOFI, SRRF, HAWK followed by single emitter fitting, HAWK followed by multi-emitter fitting. Linescans are shown below the corresponding images, averaged through the central part of the structure. (c-j) T12, located on either side of the Z-disc of muscle sarcomeres, was imaged at high-density, with low-density data being taken afterwards. (c) Low-density data analysed with single emitter ThunderSTORM. (d,e,g,h,i) High-

density data analysed with (d) multi emitter ThunderSTORM, (e) multi emitter fitting with PSF size filtering, (g) SOFI, (h) SRRF and (i) HAWK followed by single emitter ThunderSTORM fitting. Scale bar is 1μm. Only with HAWK can the doublets (ca. 160nm spacing) be clearly resolved, with the separation matching the low-density results. (f & j) show line profiles from the region indicated by the box in Figure 1c, for the images on their respective rows. (k,l,m) M8, which binds to titin domain M8 (Ig-167) and is located on either side of the sarcomeric M-band, was imaged at high-density. (k) Multi-emitter fitting with PSF size filtering, (l) HAWK followed by single emitter ThunderSTORM fitting. Scale bar is 500 nm. (m) Linescans through boxed region in l for different analysis techniques (separation is 87nm, see also Supplementary Fig. 9). To ensure reproducibility the number of frames simulated significantly oversampled the structure. Individual emitters made an expected average of 4.66 separate appearances for a mean total of 23.3 frames each. Sarcomere results are representative of 10 (T12) or 5 (M8) independent experiments.
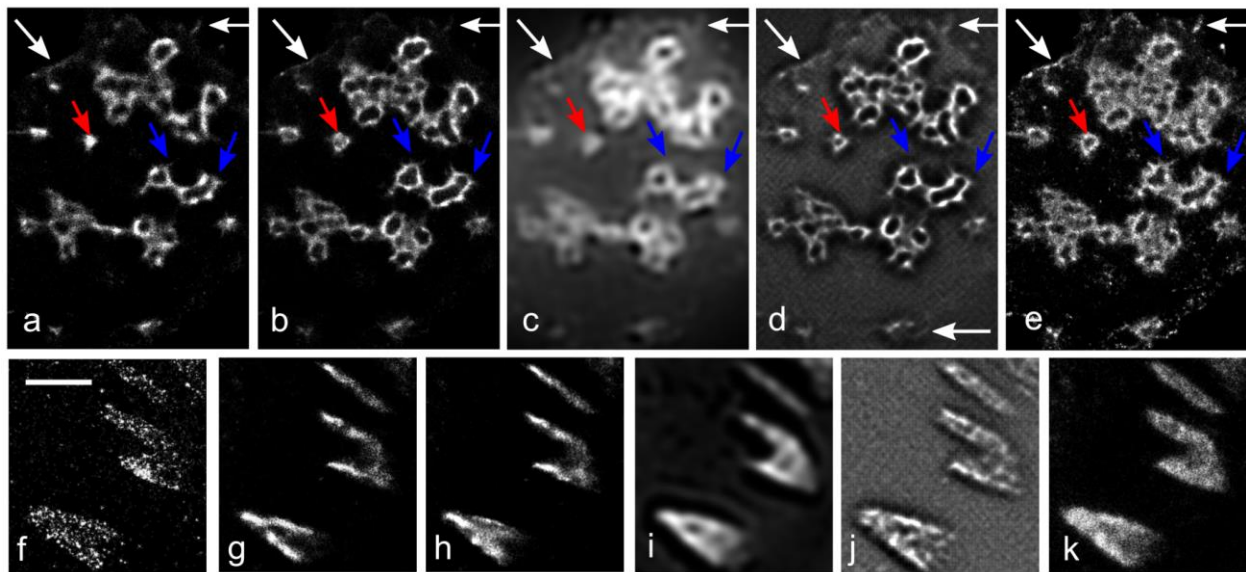

Figure 2 HAWK analysis of live cell localization yields results closer to ground truth and with better reproduction of less intense features. (a-j) Podosomes with a mEOS3.2 partial talin construct. Low-density data was taken in the switched channel (a) and high-density data in the unswitched channel (b-e). A zoom of the area indicated by a dotted rectangle in (a) is displayed in (f-j). Data was analysed with (a,f) single emitter, (b,g) multi emitter, (c,h) SOFI, (d,i) SRRF and (e,j) HAWK followed by single emitter fitting. Red and white arrows indicate parts of podosomes which are clearly present in the low-density data and HAWK analysis of the high-density data but absent in the high-density multi-emitter and SRRF analysis. The strand structure indicated by the blue arrow is changed in shape by the non-HAWK analysis methods. (k-o) Vinculin in focal adhesions labelled with mEOS2, imaged in the (k) switched (low-density) and (l-o) unswitched (high-density) channels. Data was analysed with (k) single emitter fitting, (l) multi emitter fitting, (m) 4th order SOFI, (n) SRRF, and (o) HAWK followed by single emitter fitting. The shape of the focal adhesions and background level of the images varies strongly for multi-emitter, SOFI and SRRF, with only HAWK reproducing the low-density data result accurately. Scale bar in (a) and (k) is 2 μm. Images are representative of 10 podosome and 5 focal adhesion independent experiments. Many more experiments showed greater sharpening by the other high density methods relative to HAWK but the low density data was of insufficient quality to provide an effective validation.

Online Methods

Haar Wavelet Kernel Analysis Technique: ImageJ Plugin

Below we describe the algorithm used in the ImageJ plugin, provided as supplementary software. The simulations presented in the paper were processed with an earlier version of the software also based on the Haar Tranform. This algorithm is equivalent apart from some minor edge issues, and is described in Supplementary Note.

The first three Haar kernels are of size 2, 4 and 8 respectively and are given by:

$H_0 = [1, -1]$
$H_1 = [1, 1, -1, -1]$
$H_2 = [1, 1, 1, 1, -1, -1, -1, -1]$

We then treat each pixel independently as a time sequence. So, given an image stack ($I(x,y,t)$), for a given pixel location x,ythe time sequence is $X(t)$=I(x,y,t). We then compute convolutions of X with the kernels:

Z_0=X * H_0
Z_1=X * H_1

etc, where * is the discrete convolution operator. We do not pad X, therefore the resulting Z are shorter than X. We create the final time sequence for the pixel x,yby concatenating the various Z's:

$$Z=[Z_0(0),...,Z_0(n_0),Z_1(0),...,Z_1(n_1),...]$$

where $n_i$is the number of elements in Z_i. A fluorophore switching off will cause negative values in Z. The final step is to separate the positive and negative values into Z':

$$\begin{array}{lll} Z'(i) & = & \max(Z(i), 0) \quad \text{for i=1,2,...,n} \\ Z'(i+n) & = & -\min(Z(i), 0) \quad \text{for i=1,2,...,n} \end{array}$$

As an alternative in the plugin we also offer the option to just use the absolute value:

$$Z'(i) = |Z(i)|$$

We reassemble each of the final time sequences Z' into an image stack, then analyse each frame independently with an algorithm of the user's choice, such as ThunderSTORM.

Simulated Data:

All simulated data were produced using a custom MATLAB script. Test structures consisted of a pair of lines converging from 1210nm to 10 nm over a distance of 5.6µm ('the V'), pairs of parallel lines spaces at separations of 20, 30, 50, 70, 100, 140, 200, 280, 400 and 600nm ('the lines') and circles of the same diameters as the line spacings ('the circles'). For the lines and circles each element was separated by 2.5µm to ensure independence in the reconstruction.

For each test structure emitters were placed on a 10nm square grid, representing an even

labelling density. Individual On/Off trajectories were calculated for each emitter based on exponentially distributed On and Off times. The time step was 1/10 the camera exposure time to allow for sub single frame blinking events. A Gaussian PSF corresponding to a FWHM of 2.7 pixels and a mean brightness of 2500 photons multiplied by the proportion of the frame the emitter was in the On state was then added to each frame for each emitter, including Poisson shot and Gaussian camera noise. In all cases the simulated frame was several pixels larger than the structure on each side to prevent edge effects in the reconstruction.

The On time t_{On} was fixed at a mean of 5 frames (median 3.6 frames). Emitter density was controlled by varying the Off time t_{Off} between 5000 frames (low density) and 25 frames (very high density). The number of simulated frames was correspondingly set to maintain the total average time spent in the emitting state (256-25,600 frames). The emitter density was thus the product of the emitter duty cycle and the labelling density,

$$D_{em} = \left(\frac{1}{0.01um}\right)^2 \frac{t_{On}}{t_{Off}}$$ (12)

which varied from 10 – ca. 1000 emitters / μm^2 for the parallel lines and circles and was ca. 2000 emitters / μm^2 for the converging lines (the 'V').

Experimental Data:

Experimental measurements were performed on a customised STORM microscope, built around a DMi8 Microscope body and 'SuMo' passively stabilized stage (Leica-microsystems GMBH). In this system the 1.43 160X objective (Leica-microsystems GMBH) is mounted to the underside of the stage via a piezo drive (PI). Diode lasers of 638nm (Vortran), 561nm (Oxxius) 473nm (Dragon Laser) and 405nm (Vortran) as appropriate were depolarised through optic fibres, combined, apertured and expanded to pass through the objective and provide TIRF illumination. The TIRF beam reflected back through the objective was picked off with a half mirror and imaged on a 128 photo-diode micro array (RS). The signal was digitised and centroided by a micro-controller (Arduino). Focus drift caused displacement of the reflected beam on the array. This drift was monitored and corrected for using the piezo drive.

Fluorescence was split according to wavelength by an image splitter (Photometrics Dual-view / OptoSplit II CAIRN Research) and imaged side by side on a fast EMCCD camera (Photometrics Evolve). For the fluorescent proteins mEOS 2 and mEOS 3.2 filter windows used were 500-530nm for the unconverted channel and 575-630nm for the photo-converted channel. For mEOS 2 high density data was collected in the unconverted channel while low density data was collected simultaneously in the converted channel. For mEOS 3.2 the 473nm laser used for excitation of the unconverted state caused too much photo conversion for simultaneous low density acquisition so the data sets were taken sequentially. Approximately 2500 of a total of 15,000 (podosomes) or 10,000 (focal adhesions) frames were used for the high density data (shown in Figure 2) as this produced images with very good signal-to-noise ratios. However, when the frame number was reduced to 400 the features were still clear and the resolution (as measured with FRC) was not greatly reduced (e.g. from 63nm to 72nm for the focal complex data shown in Supplementary Figure 15). Acquisition time was limited to 150s to avoid sample remodelling during acquisition.

For Alexa647 and Atto647N only one channel was used, transmitting 660-700nm. Exposure time was 10 ms and the pixel size was 100nm. For Atto647N the density was controlled by allowing significant photo-bleaching between high density and low density acquisitions (10,000 frames each).

The imaging of AF647 M8 sarcomere samples was performed in a standard reducing

buffer (Glox-glucose,200mM MEA). The emitter density was controlled with 405nm excitation, with 2000 10ms frames acquired. Increased photo-bleaching with this dye over ATTO647N prevented high quality low density data from being acquired on the same structure. Low density data was produced from a 10-20 thousand frame sequence with no 405nm activation once photo-bleaching had sufficiently reduced the emitter density.

DNA origami structures labelled with AF647 or ATTO647N at a separation of 50nm (STORM nanorulers GATTAQuant Gmbh.) were prepared and attached to 35mm glass dishes (Greiner Bio-One) using a BSA-biotin (Bio-vision) – neutravidin (Molecular probes) link according to the manufacturers instructions. Alexa647 samples where imaged in the same reducing buffer as above for 5000 20ms frames. ATTO647N samples were imaged in PBS for 5000 100ms frames. To achieve sufficient emitter density in these sparse samples continuous strong 405nm activation was used.

Super-resolution Analysis:

Simulated and experimental data were both analysed, keeping the parameters the same where possible. Some parameters had to be altered to enable optimal performance from all algorithms due to the low background level in the simulations and the the differences in the width of the PSF between simulations and experiments.

Gaussian fitting and image rendering was performed using ThunderSTORM[14]. Particle detection used the 'difference of Gaussians' filter with upper and lower sigmas of 1.0 and 1.6 (defaults) respectively. The PSF model was 'integrated Gaussian' and the estimator was 'Maximum Likelihood Estimation'. For single emitter fitting the default fitting radius of 3 pixels was used. For multi emitter fitting a radius of 5 pixels and a p value threshold of 0.05 were used as these had been determined to be the most effective in discriminating closely spaced flurophores in previous simulations[5]. For multiple emitter fitting, a maximum of five emitters per fitting region were allowed to prevent excessive false localizations and to limit computational time. Rendering of the reconstruction used 'average shifted histograms' using the default parameters with 10nm pixels (5nm for the 'lines' and 'circles'). Due to the much finer structure expected in the M8 sarcomeres and DNA origami structures ThunderSTORM reconstructions instead used the 'Normalised Gaussian' plot with a 10nm Gaussian blur and a 5nm pixel size. The SRRF settings were also changed to reflect the expected smaller separation (those described as 'MAX' in Supplementary figure 7).

SOFI analysis was performed using the 'Balanced SOFI' MATLAB script provide by the authors of the original paper (Giessbuehler *et al.*[22]), which calculates the cross cumulant up to 4th order. For simulated data either the 4th order or the 'balanced' output was chosen for display depending on which was judged to be a better reproduction of the ground truth structure. For experimental data the 'balanced' output was always chosen.

SRRF analysis[13] was performed using the 'nanoJ' plugin for ImageJ linked from the authors website (https://bitbucket.org/rhenriqueslab/nanoj-srrf/wiki/Home). For simulated data, the algorithm settings (starting from default values) were adjusted to give the most accurate reproduction of the ground truth structure with minimum sharpening and intensity artefacts for 'the V' and 'the lines', the latter using the highest density simulation. Non default settings used were 'ring radius' of 0.3, 'radiality magnification' of 10 and 'axes in ring' of 8 . For experimental data, these settings were found to increase the fixed pattern noise and background without any noticeable improvement in resolution so default settings were retained. An illustration of the different images obtained for different settings is given in Supplementary Figure 7.

3B analysis[12] was carried out using the default parameters, a 10nm super-resolution pixel size (to give a magnification of 10) and with the number of frames capped at 300 to limit computational time. A 20nm Gaussian blur was applied in the output images.

Different super-resolution algorithms produce output at varying magnification and pixel offset, and crop the edges of the image by differing amounts. Therefore bilinear interpolation (ImageJ) was applied to the lower resolution images to equalize the super-resolution pixel size where necessary.

Image sequences pre-processed using HAWK were analysed in the same way as unprocessed ones. Whether single or multi emitter fitting was used, parameters were not changed from the parameters used for non-filtered fitting. The exceptions were the 'camera offset' being set to zero, as the processing removes any background, and the filtering of localizations based on the fitted width (σ = 60-130nm for simulations and 90-150 nm for experimental data) for reasons described in Supplementary Note. For the simulated, focal adhesion and DNA origami data the first three Haar filter levels were used, whereas the denser sarcomere and podosome HAWK analysis used 5 filter levels.

Due to the small size and sparse nature of the DNA origami samples only a minority of structures showed evidence of multiple flurophores emitting simultaneously, despite strong UV activation. Structures were selected for comparison (Supplementary figures 11 &12) that showed substantial sharpening artefacts by comparing the HAWK and single-emitter reconstructions. Images were confirmed to be DNA origami structures where the measured separation between two clearly resolved 'spots' in the reconstruction where 45-55 nm and contained multiple localizations. It was also confirmed that the single emitter and HAWK localizations principally occurred at the same time point in the image sequence. These conditions were used to negate the possibility of finding an apparently resolved DNA origami structure that only contained coincidental background localizations, and select structures where the majority of flurophore appearances overlapped each other.

Precision and accuracy evaluation

The effects of HAWK on localization precision and accuracy were assessed using simulations of a single emitter making multiple reappearances and examining the distribution of localization positions. As HAWK intrinsically depends on chromophore blinking the single emitter was made to blink with the same ON and OFF times as the 1000 emitters /μm^2 simulations. The frame size was reduced to 64 by 32 pixels and the number of frames set to 25600. The emitter intensity and background light level were varied (intensity 156-2500 photons / frame, background 0-200 photons / pixel).

To assess precision, single emitter fitting was performed on both HAWK processed and unprocessed image sequences. Due to the fact that HAWK may make multiple localizations of a single emitter in a single frame, and that the increased noise can produce many extra background localizations (that have no structure, and would depend on the relative size of the background) quantitative comparison of the false positive/negative rate was not attempted. As a test for pixelation effects, some simulations were repeated for the emitter position in the corner of a camera pixel as well as in the centre. No noticeable differences in the distribution of localization positions were observed.

The bias with HAWK was assessed by repeating the simulations with a second constantly emitting emitter placed a fixed distance away in the positive x direction. The distance was varied between 20nm and 300nm for an emitter intensity of 250 photons/frame and a background light level of 25 photons/pixel. Additionally the intensity and background varied as above for the fix separation of 100nm. Hawk with single emitter fitting was compared with unprocessed multi and single emitter fitting. In the multi emitter case the parameters used were as before but the number of emitters was limited to two. Where two emitters were identified in a single frame the one with the localization with the most negative x (corresponding to the blinking emitter) was selected from the localization list to be included in the analysis. This disregards all the frames where both

the emitters were on and the algorithm mistakenly produces a single localization at their centre (responsible for artificial sharpening). For unprocessed single emitter fitting, only frames where both emitters where known to be emitting from the original simulation where included. Where possible the x and y coordinate distributions were fitted to Gaussian functions, the precision measured as the FWHM and the bias as its central location. This was not possible for the multi emitter data at separations over 100nm as the distributions contained highly skewed or multiple peaks. So for the distance variation simulations the mean and standard deviation (converted to a FWHM by multiplying by 2.355) were instead used to measure the bias and precision respectively.

Simulation of drift

The microscope used for experimental data acquisition features both passive and active stabilisation and displays very low sample drift compared to a more conventional system. To ascertain the effects of drift with and without HAWK, simulated drift was added to the image sequence of some of the simulated and experimental data (333 emitters / μm^2 'lines' and T12-sarcomere). The image sequences were expanded in size in the x direction to accommodate the size of the drift. The space was filed with Gaussian noise that reflected the measured background level in each case. MATLAB was used to expand each frame by a factor of x10 (without interpolation) in x and cyclically permuted the required number of pixels to induce the relevant time dependent drift before being resized back again. This resulted in the original image drifting linearly across the larger image frames. The unprocessed data were analysed using single emitter fitting and ThunderSTORM's inbuilt cross correlation based drift correction routine. The parameters chosen ('magnification' x2, 'slices' 20) were those that best reproduced the known drift. The estimated drift parameters were saved for import into the HAWK processed localizations. HAWK was then applied to the drift sequences followed by single emitter fitting. In order to apply the pre-established drift correction the frame number associated with each localization had to be reassigned to the frame of the original sequence that it corresponded to. The pre-establish drift parameters without HAWK were applied and the reconstruction produced in the previous way. The drift velocity was varied from 0.2 to 3.13 nm/frame and compared with no drift.

Out of focus background

To simulate an out of focus background a random distribution of emitters with the same brightness and blinking properties was added to the 10nm grid used in the previous simulations at a mean density of 1 position in 10. Each background emitter had a random z height between 0 and 1μm whereas all the structural emitters had a z height of 0. The PSF of the background emitters were appropriately broadened according to their distance from the focal plane that was positioned at z=0 .

FRC measurements

Measurements of the FRC resolution were performed using the BIOP FRC plugin (https://imagej.net/Fourier_Ring_Correlation_Plugin) for ImageJ. The correlation threshold was fixed at 1/7th. For the localization based methods that produce a list of localizations, this list was randomly split into two and an image produced from each as the input to the FRC measurement. For SOFI and SRRF that only produce an output image, the initial sequence was divide into odd and even frames and analysed separately thus providing the two independent input images required. The HAWK processed results had to be analysed differently. The Longer time scale Haar wavelet filters can produce several frames containing an image of an emitter in a single frame or the original sequence. This repeated localization of the same emitter would increase the

degree of correlation between the two input reconstructions, artificially improving the measured resolution. To remove these duplications of a single localization, the output of each filter level was analysed separately with the frame numbers reordered to match the original input. A single 'true' localization should then appear in each sub sequence in adjacent frames up to the length of the Haar wavelet used (ie $2^{(m-1)}$) if they were sufficiently bright. Gaussian fitting was performed using ThunderSTORM on each filter level separately and duplicates were merged in the localization table using the inbuilt function if their positions were within the localization precision of each other and 'ON' for up to the length of the filter (i.e. 1 frame for level 1, 2 frames for level 2, 4 frames for level 3 etc.) with no 'OFF' frames between. The results of each level concatenated to produce an output localization table that could be split as above to produce two input images for the FRC calculation. In all the localization based cases the measurement was repeated three times and the average and standard deviation taken.

Sarcomere Samples:

Rabbit and mouse psoas or cardiac myofibrils were prepared essentially as described (Knight, 1982; Cornachione et al., 2015)[23,24] and stored in rigor buffer (140 mM KCl, 2 mM MgCl$_2$, 1 mM EGTA, 20 mM HEPES, pH 6.8, containing protease-inhibitors (Roche)). Suspensions of myofibrils in rigor-buffer were applied to poly-lysine coated glass-bottomed dishes and fixed with 4% PFA in rigor buffer, washed in PBS and incubated in PBS/10% normal goat serum before incubating with mouse monoclonal antibody T12 (binding to an epitope near the N-terminus of titin), which labels the fibrils at the Z-disc. Alternatively, myofibrils were labelled with a rabbit polyclonal antibody against titin M8, which labels the C-terminal end of titin at the sarcomeric M-band. Goat anti-mouse or anti-rabbit secondary antibodies conjugated to Atto647N (50185, Sigma) or Alexa647 (A-21244, Life Technologies) were applied after washing the samples in PBS, and visualisation performed after washing away unbound secondary antibody with PBS.

Podosome Samples:

mEOS3.2 sequence was amplified from a template (gift from Dylan Owen, King's College London) using PCR and cloned into an pLNT/Sffv-MCS vector via pCR Blunt vector (Invitrogen). A cDNA encoding residues 1975-2541 of human talin was amplified using PCR from a template plasmid we previously generated.[25] This sequence was then cloned via pCR Blunt vector into the multiple cloning site of the pLNT/Sffv-mEOS3.2-MCS vector generating the mEOS3.2-talin (1975-2541) lentiviral expression construct. VSV-G pseudotyped lentivirus encoding mEOS3.2-talin (1975-2541) was packaged in HEK-293T cells by transient transfection of the cells with the p∆8.91 and pMD.G accessory plasmids along with the pLNT/Sffv transfer vector. Supernatants containing lentivirus were harvested after 48 h and filtered through a 0.45 µm filter. THP-1 cells (ATCC® Cat. no. TIB-202™) were incubated with lentiviral supernatants in 12-well plates for 24 h and washed thoroughly. The cultures were then expanded in 37℃, 5% CO2 in RPMI-1640 medium (R0883, Sigma) supplemented with 10% heat-inactivated FBS (SV30160.03, GE Healthcare), 1% penicillin/streptomycin (P0781, Sigma), and 0.05 mM β-mercaptoethanol (125472500, ACROS). For imaging, 35 mm dishes with #1.5 glass coverslip bottom (WPI, FL) were coated with 10-15 µl/ml bovine fibronectin (F1141, Sigma) in PBS for 3 hours at 37℃. After 2x wash with PBS, $6x10^5$ cells were seeded on each dish with 2 ng/ml recombinant human TGF-β (240-B, R&D Systems). The cells were incubated for 16-24 hours, and the medium was changed to RPMI-1640 without phenol red (R7509, Sigma) supplemented with 10% FBS before imaging.

Focal adhesion samples:

For transient expression of mEOS2-vinculin, HeLa cancer cells were transfected with Effectene Transfection Reagent (Qiagen) according to the manufacturer's instructions. Cells were seeded in 24-well plates the day before transfection. The next day, cells were transfected and incubated over night with the transfection mixture. Thereafter, transfected cells were harvested, washed and reseeded in 35mm glass-bottom imaging dishes (Greiner) and cultured for another 24 hours. Before live imaging, the medium was replaced with HEPES containing Optimem (Life Technologies. Paisley, UK) supplemented with 10% FBS.

SIM and iSIM measurements

HeLa cells were seeded on 35 mm dishes with #1.5 glass coverslip bottom (WPI, FL) ~5×10^4 cells per dish. After leaving to adhere for 16 hours, the cells were fixed for 20 minutes in 3.6% formaldehyde, permeabilised for 5 minutes in 0.1% Triton X-100, and blocked in 3% BSA for 30 minutes. The anti-tubulin antibody (T8328, Sigma) was added diluted 1:200 in PBS with 3% BSA, and incubated for 1 hour. An Alexa-647 conjugated secondary antibody (A21235, Invitrogen) was diluted to 1:500 in PBS with 3% BSA and incubated for 30 minutes.

Experimental measurements were performed at the Nikon Imaging Centre at King's College London. Several images were acquired on commercial SIM and iSIM instruments following the manufactures recommended protocols. In all cases a pair of images on the same region of the sample were acquired sequentially for input to the FRC calculation. FRC measurements were performed as above and the average for each machine taken with results comparable to the manufacturers specifications.

Data availability statement

Supporting data can be downloaded from the KCL server. https://dx.doi.org/10.18742/RDM01-318

Code availability statement

The HAWK ImageJ plugin is available as Supplementary Software.
Updates are available from www.coxphysics.com

Ethical regulations for animal use statement

The use of animal tissue described in the paper was covered by the KCL institutional licence for tissue only animal studies.

References (Online Methods)

22 Geissbuehler, S. et al. Mapping molecular statistics with super-resolution optical fluctuation imaging (bSOFI). *Optical Nanoscopy* **1**(4) (2012)

23 Knight, P.J. and Trinick, J.A. Preparation of myofibrils. *Meth. Enzymol.*, 1982. **85**: p. 9-12.

24 Cornachione, A.S., Leite, F.S., Bagni, M.A., and Rassier, D.E. The increase in non-cross-bridge forces after stretch activated striated muscle is related to titin isoforms. *Am J Physiol Cell Physiol*, 2015. DOI: https://doi.org/10.1152/ajpcell.00156.2015

25 Vijayakumar, V. Tyroine phosphorylation of WIP releases bound WASP and impairspodosome assembly in macrophages. *Journal of Cell Science*, **128**(2):251-265, 2015.